Kinematic analysis of a planar manipulator with anti-parallelogram joints and offsets

Philippe Wenger, Matthieu Furet

Kinematic analysis of a planar manipulator with anti-parallelogram joints and offsets

Philippe Wenger[1] and Matthieu Furet[1,2]

[1] Laboratoire des Sciences du Numérique de Nantes (LS2N), CNRS, 44321 Nantes, France
[2] Ecole Centrale de Nantes, 44321 Nantes, France

Abstract. Industrial robotic manipulators mostly use revolute or prismatic joints. In this paper, an anti-parallelogram mechanism, referred to as *X-joint*, is considered as an alternative choice to a revolute joint in the kinematic design of robots. This choice lends itself well to a remote actuation with cables, which contributes to lower inertia. We show that replacing revolute joints with X-joints in a planar 2-dof manipulator improves drastically the size of the workspace in the presence of joint limits. On the other hand, the kinematic analysis becomes significantly more difficult, owing to the much more complicated algebra involved in the input/output equations. The inverse kinematics, the singularities and the workspace optimization are investigated. A tentative design of a 2-X planar linkage is proposed and compared to its 2-R counterpart.

Keywords: Anti-parallelogram joint, Inverse Kinematics, Singularity, Workspace, Optimal Design

1 Introduction

An anti-parallelogram mechanism, referred to as *X-joint* in this paper, has two opposite pairs of equal-length bars like in the parallelogram joint, but contrary to this latter, the bars of one pair cross each other. The X-joint is less popular than the parallelogram joint and, as far as we know, it has never been used in industrial robots. It can be found in knee [1] and bird neck models [2], in gear trains [3] or in tensegrity mechanisms [4],[5],[6],[7],[8]. In [2], [7] and [8], the X-joints were arranged in series and adjacent to each other to form planar manipulators, as shown in figure 1, left. In this paper, an offset is added between two successive X-joints and between the last X-joint and the reference point P, like in figure 1, right. The use of X-joints is suitable for a remote actuation with cables [2], [8], an interesting choice for a lightweight design. As it will be shown further, moreover, X-joints can generate much larger workspaces than R joints. On the other hand, it turns out that the inverse kinematics of such a manipulator becomes much more complicated. When two X-joints are adjacent as in figure 1, left, it was shown in [9] that the inverse kinematics can be solved with a quartic polynomial and admits up to four solutions. When offsets are added, it turns out that the degree of the inverse kinematics polynomial is twice higher, as shown

further. In the next section, the inverse kinematics of a 2-dof planar manipulator with X-joints and offsets is derived and the singularities as well as the workspace boundaries in the absence of joint limits are determined. Then, the effect of joint limits is analyzed. Finally, a comparative workspace-based study is carried out between a classical 2-R planar manipulator and a 2-X manipulator with offsets.

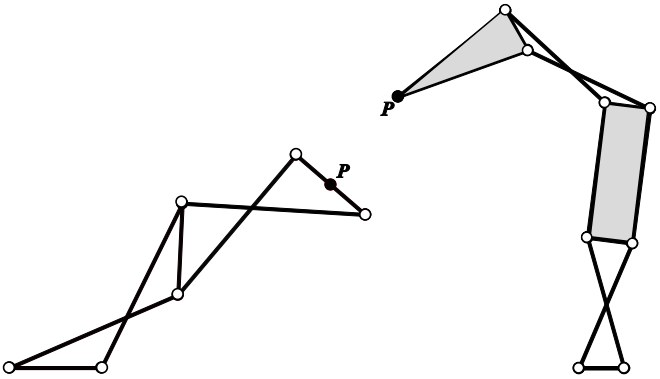

Fig. 1: A 2-X manipulator with no offsets *(left)* and with offsets *(right)*.

2 Manipulator studied

The manipulator studied consists of two identical X-joints and two offset links in series as shown in figure 2. Each X-joint i has a base bar and an upper bar of length b and two crossed bars of length L with $L>b$. The two links are defined as a rectangle and a isoceles triangle, respectively. The rectangle, of height h, links the two X-joints while the triangle, of altitude h, links the second X-joint and the reference point $P = (x, y)$. The reference frame is centered at the middle of the base bar with the x-axis horizontal and pointing to the right. Let α_i define the orientation of the upper bar of the i^{th} X-joint w.r.t. its base bar. For a matter of completeness in the kinematic analysis, each X-joint is assumed to move within its full range. In this case, $-2\pi < \alpha_i < 2\pi$. Thus, α_i cannot define the mechanism configuration unambiguously. Let l_i be the length of the line segment that links the middle points of the top and base bars of each X-joint i (shown in red dotted line in figure 2). The angle between this line and the direction orthogonal to the base bar is referred to as θ_i. It is easy to verify that $\alpha_i = 2\theta_i$. When $-\pi < \theta_i < \pi$, thus, the mechanism makes a full turn and the manipulator configuration can be defined by (θ_1, θ_2). Two more angle parameters are introduced, namely, ϕ_1 and ψ_2, which define the angle of the left crossed-bar of the first X-joint and the angle of the right crossed-bar of the second X-joint, respectively (see figure 2). These angles are useful for the derivation of the inverse kinematics. The length l_i of the line segment that links the middle points of the top and base bars can

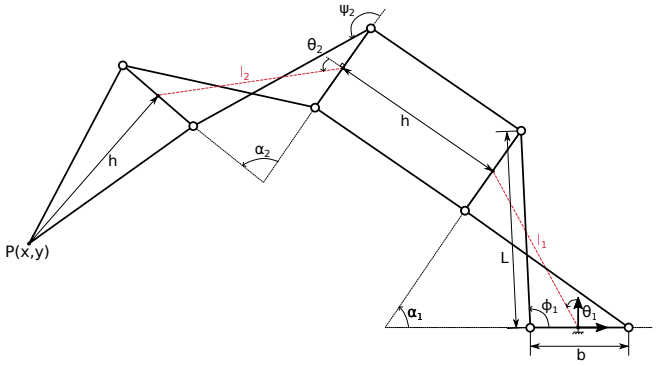

Fig. 2: Manipulator description.

be expressed as follows [2]:

$$l_i(\theta_i) = \sqrt{L^2 - b^2\cos^2(\theta_i)} \tag{1}$$

3 Direct and inverse Kinematics

The direct kinematic equations of the manipulator studied are obtained upon expressing the Cartesian coordinates (x, y) of the reference point in the base frame:

$$\begin{cases} x = -h(\sin(2\theta_1) + \sin(2\theta_1 + \theta_2)) - l_1(\theta_1)\sin(\theta_1) - l_2(\theta_2)\sin(2\theta_1 + \theta_2) \\ y = h(\cos(2\theta_1) + \cos(2\theta_1 + \theta_2)) + l_1(\theta_1)\cos(\theta_1) + l_2(\theta_2)\cos(2\theta_1 + \theta_2) \end{cases} \tag{2}$$

where $l_1(\theta_1)$ and $l_2(\theta_2)$ are defined in (1).

The inverse kinematics is usually established after deriving the so-called characteristic polynomial, a univariate polynomial in one of the input variables that is obtained from the direct kinematics equations. It is not convenient here to combine the two equations in (2) to obtain this polynomial because of the presence of square roots. These square roots would have to be first cleared out, thus doubling the degree of the resulting polynomial and yielding extraneous roots. Instead, we proceed like in [9] by writing x and y as functions of the crossed-bar angles ϕ_1 and ψ_2 as follows:

$$\begin{cases} x = \frac{b}{2}\cos(\alpha_1 + \alpha_2) + L\cos(\phi_1) + L\cos(\psi_2 + \alpha_1) - h\sin(\alpha_1) + h\sin(\alpha_1 + \alpha_2) - \frac{b}{2} \\ y = L\sin(\phi_1) + L\sin(\psi_2 + \alpha_1) + h(\cos(\alpha_1) + \cos(\alpha_1 + \alpha_2)) + \frac{b}{2}\sin(\alpha_1 + \alpha_2) \end{cases} \tag{3}$$

The loop closure equations of the two X-joints are then added:

$$\begin{cases} -2Lb\sin(\alpha_1)\sin(\phi_1) - 2Lb(\cos(\alpha_1) + 1)\cos(\phi_1) + 2b^2(\cos(\alpha_1) + 1) = 0 \\ 2Lb\sin(\alpha_2)\sin(\psi_2) + 2Lb(\cos(\alpha_2) + 1)\cos(\psi_2) + 2b^2(\cos(\alpha_2) + 1) = 0 \end{cases} \tag{4}$$

A set of four equations in four unknowns is thus available. A univariate polynomial can be obtained upon elimination of three of the four unknowns, which is done here with the *Projection* function of the *Maple Siropa* library [9], [10]. This function projects the system of four equations in order to obtain one single equation in one single variable, chosen here as ϕ_1. The half-tangent substitution yields a factored polynomial, one of which defines the characteristic polynomial. Interestingly, the characteristic polynomial obtained turns out to be of degree 8 in t=tan($\phi_1/2$), leading to the possible existence of eight inverse kinematic solutions. Note that this degree was only four for the 2-X manipulator with no offsets and a maximum of four inverse kinematic solutions were found [9]. The expression of the 8-degree polynomial is very large and cannot be displayed here. It can be found in a technical report [11]. The inverse kinematic solutions are obtained by solving in cascade the first equation in (4) and the two equations in (3), following the same as process as in [9].

The inverse kinematics is solved for a 2-X manipulator of dimensions $L = 1/2, h = 1$ and $b = 1/3$ at $x = 0$ and $y = 9/10$. Eight solutions are found (see figure 3). It is worth noting that these eight solutions exist as long as no restriction is imposed on the rotation range of the X-joints, i.e. $-\pi < \theta_i < \pi$. When $-\pi/2 < \theta_i < \pi/2$, for example, it can be verified that the only solutions are those two symmetric configurations furthest to the right and left (in purple and pink in figure 3).

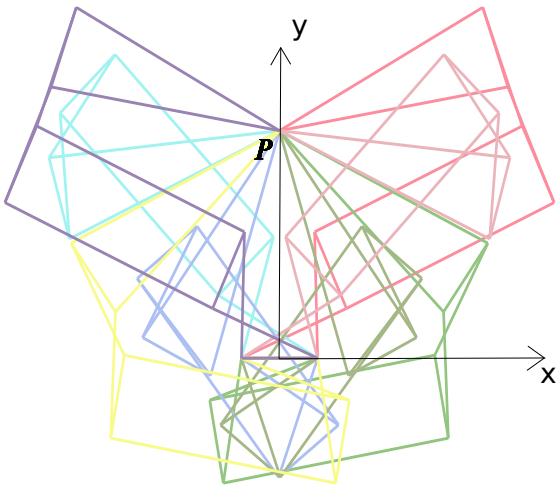

Fig. 3: The eight solutions at $x = 0$, $y = 9/10$ ($L = 1/2, h = 1$ and $b = 1/3$).

4 Singularity and workspace analysis

The Jacobian matrix of the manipulator can be derived from system (2). Its determinant is calculated to plot the singularity curves in the joint space. After

a careful inspection of a great number of plots, it turns out there are six, four or two curves depending on the link dimensions. Figure 4 shows the singularity plots when $b = 1/3$, $h = 1$, $L = 1$ (left) and $L = 2$ (right).

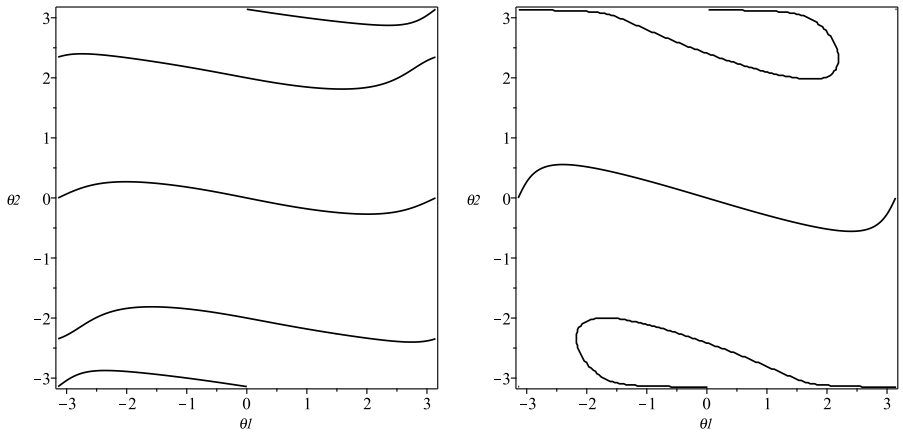

Fig. 4: Singularity curves in the joint space when $h = 1$, $b = 1/3$: there are four curves when $L = 1$ *(left)* and two curves when $L = 2$ *(right)*.

In the absence of joint limits, the workspace boundaries are defined by the graph of the discriminant of the characteristic polynomial. A huge polynomial containing 2905 monomials and of degree 32 in x and y is obtained. Figure 5 shows the workspace boundaries for a manipulator with link dimensions $b = 1/3, h = 1, L = 1/2$ (left) and $L = 1$ (right). Internal boundaries divide the workspace into constant accessibility regions. Accessibility can be obtained in each region upon choosing an arbitrary point and solving the inverse kinematics. The number of solutions is indicated with colors as explained in the figure legend.

We now study the workspace when the rotation range of each X-joint is defined by $-\pi/2 < \theta_i < \pi/2, i = 1, 2$. These joint limits are necessary to avoid the flat singularities of the anti-parallelograms and to allow a remote actuation with cables. This time, the workspace boundaries are plotted upon mapping into the (x, y) plane the joint space singularity curves as well as the joint space boundaries. Figure 6 shows the resulting workspace boundaries when $b = 1/3$, $h = 1$, $L = 1$ and $-\pi/2 < \theta_i < \pi/2$.

The manipulator has one (resp. two) solutions in the light-grey (resp. dark-grey) areas, respectively. The height of the void Y_{vh} can be determined easily as it is bounded by the curves defined by the joint limits. More precisely, the upper point of the void is reached when $\theta_2 = \pi/2$ and $x = 0$. Solving $x = 0$ for θ_1 in the first equation of (2) and replacing the obtained solution into the second equation of (2) yields $Y_{vh} = \sqrt{3L^2 - b^2}$. Interestingly, the height of the void is independent of h. The void cannot be removed since b must be lower than L, but

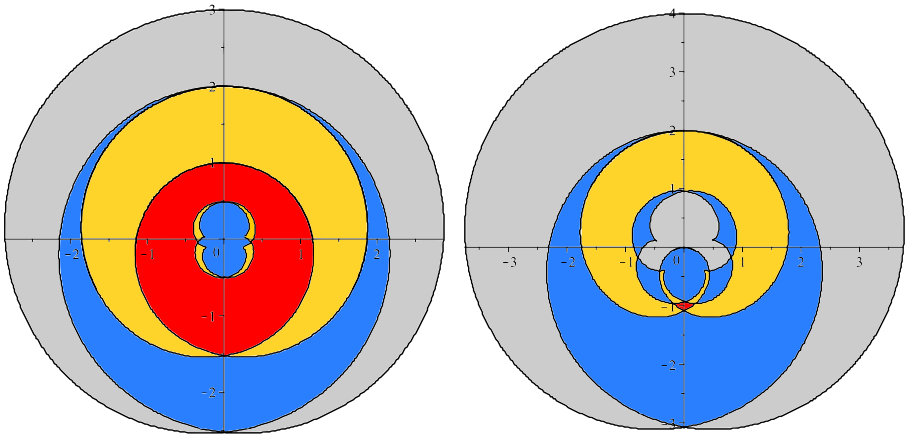

Fig. 5: Workspace when $h = 1$, $b = 1/3$ and $L = 1/2$ *(left)*, $L = 1$ *(right)*. Number of solutions is 2 (resp. 4, 6, 8) in the areas filled in grey (resp. blue, yellow, red).

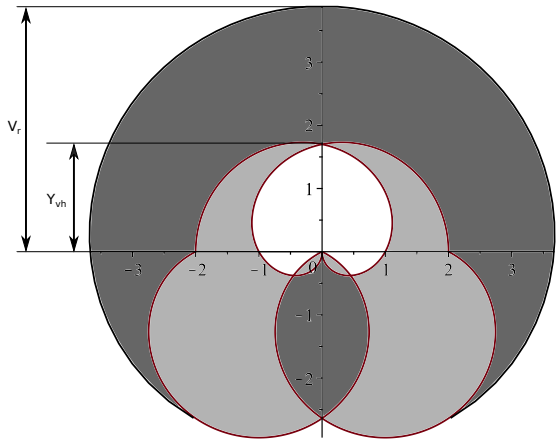

Fig. 6: Workspace when $b = 1/3$, $h = 1$, $L = 1$ and $-\pi/2 < \theta_i < \pi/2$. Light-grey (resp. dark grey) areas have 1 (resp. 2) inverse kinematic solutions.

it can be minimized when L and b are small and b is small w.r.t. L. The vertical maximal reach V_r of the manipulator is equal to $V_r{=}2h+2\sqrt{L^2-b^2}$. So to have a large maximal reach, knowing that L and b should be small, h should be chosen high. Suppose that the desired maximal reach is $V_r = 2$. Figure 7, left, shows the workspace of a suitable design ($b = 0.05$, $h = 0.91$, $L = 0.1$), exhibiting a void of height $Y_{vh} = 0.166$, which is twelve times less than the maximal reach. Note that, in addition, the accessibility is equal to two almost everywhere. It drops to one only in the two symmetric curved strips located in the negative values of y and around the void. For a matter of comparison, the workspace of a 2-R manipulator with the same maximal reach $V_r = 2$ (link lengths $L_1 = L_2 = 1$) and the same joint limits ($-\pi/2 < \theta_i < \pi/2$) is shown in figure 7, right. The chosen joint limits would allow a remote actuation with cables for both manipulators. It is apparent that the workspace of the 2-R manipulator is much smaller and the accessibility is equal to two only in the upper region of the workspace.

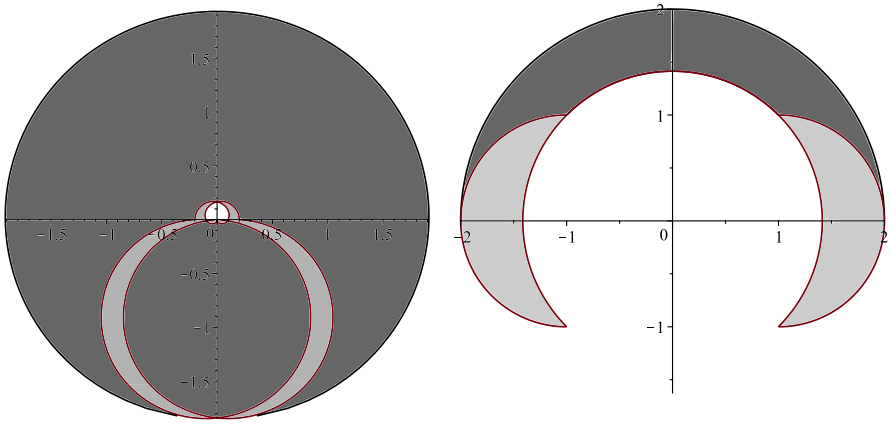

Fig. 7: Workspace of a 2-X (*left*, $b = 0.05$, $h = 0.91$, $L = 0.1$) and 2-R (*right*, $L_1 = L_2 = 1$) manipulator designed for a maximal reach equal to two.

5 Conclusion

A new family of manipulators with two anti-parallelogram joints and offset links has been considered as an alternative design to classical 2-revolute-jointed linkages. At the price of more complex input/output equations and singularity expressions, 2-X manipulators have been shown to offer a much larger workspace in the presence of joint limits. Moreover, they lend themselves well to a remote actuation with cables, which make them good candidates to lightweight designs suitable for safe interactions. In future work, a comparative study between 2-R

and 2-X manipulators actuated with cables will be performed on the basis of their wrench-feasible workspace.

Acknowledgement This work was conducted with the support of the French National Research Agency (AVINECK Project ANR-16-CE33-0025).

References

1. A. Hamon, Y. Aoustin, S. Caro, Two walking gaits for a planar bipedal robot equipped with a four-bar mechanism for the knee joint, Multibody System Dynamics 31 (3), pp 283-307, 2014
2. M. Furet and P. Wenger, Kinetostatic analysis and actuation strategy of a planar tensegrity 2-X manipulator, ASME Journal of Mechanisms and Robotics, 1-19, https://doi.org/10.1115/1.4044209, 2019
3. X. Zhang,D. et al., Use of Anti-parallelogram Linkage Mechanism and Ordinary Gear Train for Power Transmission on a Rotary Engine, Proc. Third Int. Conf. on Mechanic Aut. and Control Eng., July 2012
4. M. Arsenault and C. M. Gosselin, Kinematic, static and dynamic analysis of a planar 2-dof tensegrity mechanism, Mech. and Mach. Theory, Vol. 41(9), 1072-1089, 2006
5. P. Wenger and D. Chablat, Kinetostatic analysis and solution classification of a class of planar tensegrity mechanisms, Robotica, Vol. 37, 7 July 2019, pp. 1214-1224.
6. Q. Boehler et al., Definition and computation of tensegrity mechanism workspace, ASME J. of Mechanisms and Robotics, Vol 7(4), 2015
7. S. Chen and M. Arsenault, Analytical Computation of the Actuator and Cartesian Workspace Boundaries for a Planar 2-Degree-of-Freedom Translational Tensegrity Mechanism, Journal of Mech. and Rob., Vol. 4, 2012
8. D. L Bakker et al., Design of an environmentally interactive continuum manipulator, Proc.14th World Congress in Mechanism and Machine Science, IFToMM'2015, Taipei, Taiwan, 2015
9. M. Furet, M. Lettl, P. Wenger, Kinematic analysis of planar tensegrity 2-X manipulators, Proc. 16th Int. Symp. on Advances in Robot Kinematics, Bologna, Italie, 2018
10. F. Rouillier et al., Siropa Library V1, IDDN.FR.001.140015.000.S.P.2017.000.20600.
11. M. Furet and P. Wenger, Inverse kinematics of 2-X manipulators with offsets, Technical report, LS2N-CNRS, 2019.